

## Correspondence

A two-stage detector is proposed to accommodate high computational load requirements of modern radar systems. The first stage of the proposed system is a low-complexity detector that operates at an unusually high false alarm probability value around 1/10. This stage is to prescreen and eliminate some of the test cells with relatively few operations. The second stage operates only on the cells passing the prescreening stage and implements a high-complexity detector at a desired system false alarm rate. Due to the detector cascade, the second stage has a large amount of computational load reduction, on the order of 10 folds, in comparison with the single-stage systems. The mathematical analysis of the described two-stage detector is presented, and the relations for the false alarm and detection probability are derived. The numerical results show that it is possible to achieve a significant computational load reduction at a negligible performance loss with the proper selection of detector parameters.

### I. INTRODUCTION

Surveillance radars continuously scan the environment and process the stream of incoming data to decide on the presence or absence of targets in the region of interest [1, 2]. Modern systems operate at increasing range and angular resolutions, which leads to increasing computation load requirements on the processor. In this correspondence we present a two-stage detection system which is aimed to reduce the computational-load requirements of modern radar systems [3].

A typical radar system declares relatively few target-present decisions and an overwhelming number of target-absent decisions in unit time. The detector of a typical system executes the same set of instructions on each test cell for target detection. Therefore, the detector unit can be said to have very poor efficiency when one considers the amount of total computational power used per target present decision. The main idea of the present correspondence is to reduce the overall load of the detector by eliminating some of the incoming cells with a low-complexity

Manuscript received August 2, 2011; revised January 30, 2012; released for publication April 27, 2012.

IEEE Log No. T-AES/49/1/944372.

Refereeing of this contribution was handled by F. Gini.

---

0018-9251/13/\$26.00 © 2013 IEEE

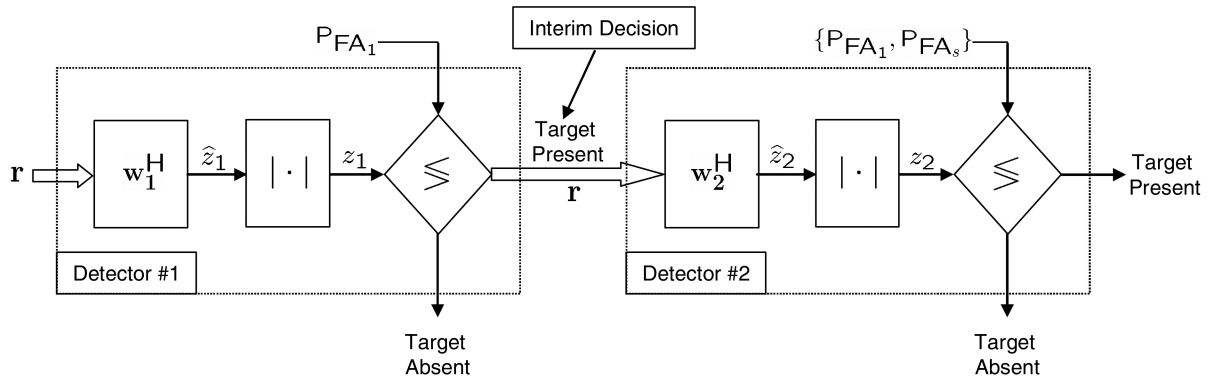


Fig. 1. Proposed two-stage detector. Detector 1 is simple detector operating at unusually high  $P_{FA}$  values, say 1/10. Detector 2 is a high-complexity detector with good clutter suppression and operates at standard  $P_{FA}$  values.

prescreening unit. It should be noted that in addition to the computational-load reduction, the drop in the sheer number of cells to be examined by the main processor can also enable the designer to overcome some other system bottlenecks, as described below.

A concrete application example for the proposed detector can be given as follows. A radar system with a rotary antenna is considered. The system utilizes coded waveforms, has the range resolution of  $\Delta R = 10$  m, has 10 antenna elements lined in the elevation direction, and each antenna element is sampled with  $T_c = 2\Delta R/c = 0.667$  ns (one sample per chip) and quantized at 15 bits/sample. A simple calculation shows that this system produces a data rate of 4.5 Gbits/s. The rapid (low latency) and reliable transfer of data collected by a rotary antenna unit to the main processor becomes a significant problem on its own for high-resolution systems. An option for the data transfer is the fiber optical slip ring structure which is an opto-mechanical component capable of transmitting 3–5 Gbits/s per optical channel. Note that if the range resolution of the described system is halved or if the number of antenna elements is doubled or by simply switching to the double chip rate operation, the data rate of the mentioned system doubles to 9 Gbits/s, and it becomes necessary to utilize more than one optical channel, which may pose additional design difficulties. In this correspondence we suggest using a new detection scheme, the two-stage detector, to overcome the bottlenecks in communication throughput and computational requirements.

With the adoption of the proposed detector, the data rate through the slip ring and the computational load of the main processor can be significantly reduced. The first stage of the proposed detector can be implemented in the rotary antenna unit (before the slip ring), and this stage can be set to operate at the false alarm rate of, say, 1/10. Since only the cells that are declared as suspicious by the first stage are processed with the second stage, the data rate through the slip ring and the computational load of the main

processor is immediately reduced by 1/10. Such a large reduction in the requirements can significantly relieve the design of high-resolution systems.

Figure 1 shows the flow diagram of the proposed system. The vector  $\mathbf{r}$  is the input representing the data collected from a range cell of interest. The linear combiners for the clutter suppression/target detection are denoted by  $\mathbf{w}_1^H$  and  $\mathbf{w}_2^H$  [4, 5]. The first detector has a low processing gain but operates at an unusually high false alarm probability  $P_{FA1} \approx 1/10$ . The data associated with the target-absent decisions of the first stage are immediately discarded; the rest is fed into the second stage for further processing.

It should be clear that a target-present decision is made only if a cell passes through both first and second stages of the proposed system. Hence, the cells discarded by the first stage can lead to the suppression of the detection probability. In this correspondence we examine the amount of probability suppression and show that the amount is indeed tolerable if the parameters of the system are suitably selected. Some other side benefits, such as the reduction in the communication data rate and the operation with partial beamforming gain, are further discussed in the numerical results section.

## II. TWO-STAGE DETECTOR

In this section we present the probability density function (pdf) of the decision statistics under target-absent ( $H_0$ ) and target-present ( $H_1$ ) hypotheses. We assume that the clutter at an individual range cell is Gaussian distributed, as in [6], [7], [8]. The extension of the present study to the non-Gaussian clutter models, such as the ones that model the sea clutter, warrants further investigation.

The signal at the input side of detector 1 can be written as follows:

$$\mathbf{r} = \alpha_s \mathbf{s}_\phi + \sigma_c \mathbf{c} + \sigma_w \mathbf{w}. \quad (1)$$

The elements of  $N \times 1$  column vector  $\mathbf{r}$  are the returns collected from  $N$  consecutive pulses from a range cell. Here we assume that the beamforming and

fast-time matched filtering (pulse matched filtering) have already been implemented and therefore the processing gain due to the beamforming and the matched filtering has been reflected over the signal component of  $\mathbf{r}$ , which is  $\alpha_s \mathbf{s}_\phi$ . The vector  $\mathbf{s}$  represents the Doppler steering vector of the target which has the following form

$$\mathbf{s}_\phi = [1 \quad e^{j\phi} \quad e^{j2\phi} \dots e^{j(N-1)\phi}]^T. \quad (2)$$

The scalar  $\alpha_s$  is either a fixed constant (Swerling-0 target) or a circularly symmetric complex Gaussian distributed random variable with zero mean and variance  $\sigma_s^2$  (Swerling-1 target). The clutter is represented by a circularly symmetric, jointly complex Gaussian distributed vector with zero mean and covariance matrix  $\sigma_c^2 \mathbf{R}_c$ .  $\mathbf{R}_c$  is normalized to have unit values on its main diagonal and  $\sigma_c^2$  is the average power of the clutter. The electronic noise is represented by  $\mathbf{w}$ , and it is assumed to be circularly symmetric, jointly complex Gaussian distributed vector with zero mean and covariance matrix of  $\sigma_w^2 \mathbf{I}$ , where  $\mathbf{I}$  is the identity matrix.

The target-present decision is produced when the outputs of both detectors exceed their corresponding thresholds. The probability of this event can be written as  $P\{|\mathbf{w}_1^H \mathbf{r}| > \gamma_1, |\mathbf{w}_2^H \mathbf{r}| > \gamma_2\}$ , where  $\gamma_1$  and  $\gamma_2$  are the thresholds. Here,  $\mathbf{w}_k^H \mathbf{r}$  corresponds to a linear combination of the entries of  $\mathbf{r}$ .

For the linear combiner  $\mathbf{w}_1$ , we suggest the cascade of a single line canceller and Doppler processing,  $\mathbf{w}_1^H = \mathbf{s}_\phi^H \mathbf{M}_1^H \mathbf{M}_1$ . (It should be noted that this operation is equivalent to the moving target indicator (MTI) with a single line canceller [7, ch. 5.2] and can be very efficiently implemented in hardware.) The  $\mathbf{s}_\phi$  vector is the hypothesised Doppler steering vector of the target whose definition is given in (2), and  $\mathbf{M}_1$  is the matrix representing MTI operation

$$\mathbf{M}_1 = \begin{bmatrix} 1 & -1 & 0 & \dots & 0 & 0 \\ 0 & 1 & -1 & \dots & 0 & 0 \\ \vdots & \vdots & \vdots & & \vdots & \vdots \\ 0 & 0 & 0 & \dots & 1 & -1 \end{bmatrix}_{(N-1) \times N}. \quad (3)$$

The second detector is utilized less frequently than the first one and allowed to be much more complex. Here it is assumed that the second detector implements the optimal signal-to-noise-and-clutter ratio maximizing filter, which is  $\mathbf{w}_2 = (\sigma_c^2 \mathbf{R}_c + \sigma_w^2 \mathbf{I})^{-1} \mathbf{s}_\phi = \mathbf{R}_{cn}^{-1} \mathbf{s}_\phi$ , where  $\mathbf{R}_{cn} = (\sigma_c^2 \mathbf{R}_c + \sigma_w^2 \mathbf{I})$  is the clutter-noise covariance matrix.

For both detectors, the output signal to clutter-noise ratio (at the steering direction of  $\mathbf{s}_\phi$ ) can be written as follows:

$$(\text{Output SNCR})_{k,\phi} = E\{|\alpha_s|^2\} \frac{|\mathbf{w}_k^H \mathbf{s}_\phi|^2}{\mathbf{w}_k^H \mathbf{R}_{cn} \mathbf{w}_k}, \quad k = \{1, 2\}. \quad (4)$$

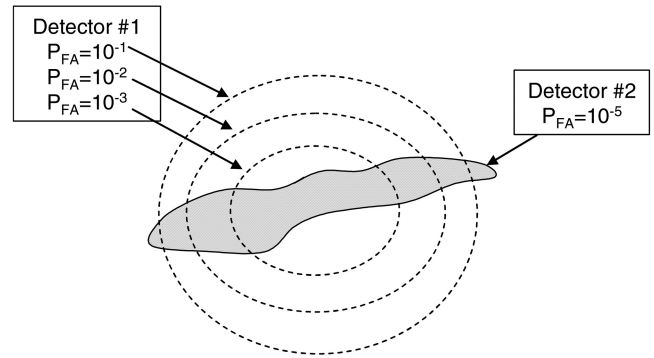


Fig. 2. Conceptual picture illustrating operation of two-stage system.

Here,  $E\{\cdot\}$  is the expectation operator. We would like to remind that the output signal-to-noise-and-clutter ratio value is the performance determining factor for the conventional single-stage detectors and that it is also critical for the proposed, two-stage system.

Figure 2 presents a conceptual picture that illustrates the operation of two detectors. Each point in this figure indicates a particular observation vector  $\mathbf{r}$ . The duty of a detector is to make a target-absent or a target-present decision for each observation vector. The area enclosed by the closed curves can be considered as the observation points for which a target-present decision is made. As expected, as the enclosed area gets bigger, the probability of detection increases, along with the probability of false-alarm. Detector 2 is the optimal Neyman-Pearson detector that encloses an area in the observation space, which maximizes the detection probability at a fixed false alarm probability (which is  $10^{-5}$  in the figure). Detector 1 is an ad-hoc detector that has less efficacy at target detection. In this figure it is pictorially shown that, by increasing the false alarm probability of the first detector to  $P_{FA} = 10^{-1}$ , we can almost cover the whole area of the optimum detector. It is clear that if the region of the optimum detector is totally enclosed by the region of first detector, then there is no loss in detection probability when two detectors are put in cascade. Our goal in this correspondence is to quantify this picture.

Different from the conventional (single-stage) detectors, the detection of a target depends on the joint distribution of  $\mathbf{z}_1 = |\mathbf{w}_1^H \mathbf{r}|$  and  $\mathbf{z}_2 = |\mathbf{w}_2^H \mathbf{r}|$ , where  $\mathbf{z}_1$  and  $\mathbf{z}_2$  are the decision statistics to be thresholded, as shown in Fig. 1. Before the derivation of the joint distribution, we introduce the intermediate  $\hat{z}_1$  and  $\hat{z}_2$  random variables:

$$\begin{bmatrix} \hat{z}_1 \\ \hat{z}_2 \end{bmatrix} = \underbrace{\begin{bmatrix} \mathbf{w}_1^H \\ \mathbf{w}_2^H \end{bmatrix}}_{\mathbf{W}^H} \mathbf{r} = \mathbf{W}^H \mathbf{r}. \quad (5)$$

In the equation above  $\mathbf{W}^H$  is a  $2 \times N$  matrix whose first and second rows are  $\mathbf{w}_1^H$  and  $\mathbf{w}_2^H$ , respectively. The random vector  $\mathbf{r}$  is jointly Gaussian distributed

with zero mean and covariance matrix  $\mathbf{R}_r$  ( $\mathbf{R}_r = \mathbf{R}_{cn}$  under  $H_0$ ,  $\mathbf{R}_r = (E\{|\alpha_s|^2\} \mathbf{s}_\phi \mathbf{s}_\phi^H + \mathbf{R}_{cn})$  under  $H_1$ ). Then, the joint distribution of  $\hat{z}_1$  and  $\hat{z}_2$  is Gaussian distributed with zero mean and covariance  $\mathbf{W}^H \mathbf{R}_r \mathbf{W}$ . The elements of the covariance matrix can be explicitly written as follows:

$$\begin{aligned} \mathbf{W}^H \mathbf{R}_r \mathbf{W} &= \begin{bmatrix} \mathbf{w}_1^H \mathbf{R}_r \mathbf{w}_1 & \mathbf{w}_1^H \mathbf{R}_r \mathbf{w}_2 \\ \mathbf{w}_2^H \mathbf{R}_r \mathbf{w}_1 & \mathbf{w}_2^H \mathbf{R}_r \mathbf{w}_2 \end{bmatrix} \\ &= 2 \begin{bmatrix} \sigma_1^2 & \rho \sigma_1 \sigma_2 \\ \rho \sigma_1 \sigma_2 & \sigma_2^2 \end{bmatrix}. \end{aligned} \quad (6)$$

The distribution of the random variables  $z_1 = |\hat{z}_1|$  and  $z_2 = |\hat{z}_2|$  can be calculated using pdf mapping for two functions of two random variables, [9, p. 19]:

$$\begin{aligned} f_{z_1, z_2}(z_1, z_2) &= \frac{z_1 z_2}{\sigma_1^2 \sigma_2^2 (1 - \rho^2)} \exp \left[ -\frac{1}{2(1 - \rho^2)} \left( \frac{z_1^2}{\sigma_1^2} + \frac{z_2^2}{\sigma_2^2} \right) \right] \\ &\times I_0 \left( \frac{z_1 z_2 \rho}{\sigma_1 \sigma_2 (1 - \rho^2)} \right), \quad z_1 \geq 0, z_2 \geq 0 \end{aligned} \quad (7)$$

where  $I_0(\cdot)$  is the modified Bessel function of the first kind and order zero. The definitions for  $\gamma_1$ ,  $\gamma_2$ , and  $\rho$  are given in (6).

The joint cumulative density function (cdf) for  $z_1$  and  $z_2$  can be written as follows:

$$\begin{aligned} F_{z_1, z_2}(z_1, z_2) &= 1 - \exp \left( -\frac{z_1^2}{2\sigma_1^2} \right) Q_1 \left( \sqrt{\frac{z_2^2}{\sigma_2^2 (1 - \rho^2)}}, \sqrt{\frac{\rho^2 z_1^2}{\sigma_1^2 (1 - \rho^2)}} \right) \\ &- \exp \left( -\frac{z_2^2}{2\sigma_2^2} \right) \left( 1 - Q_1 \left( \sqrt{\frac{\rho^2 z_2^2}{\sigma_2^2 (1 - \rho^2)}}, \sqrt{\frac{z_1^2}{\sigma_1^2 (1 - \rho^2)}} \right) \right) \end{aligned} \quad (8)$$

where  $Q_1(\cdot, \cdot)$  is the first order Marcum-Q function.

The marginal probability density and the marginal cumulative distribution function for  $z_k$  reduce to well-known Rayleigh distributions [8]:

$$f_{z_k}(z_k) = \frac{z_k}{\sigma_k^2} \exp \left( -\frac{z_k^2}{2\sigma_k^2} \right), \quad z_k \geq 0, \quad k = \{1, 2\} \quad (9)$$

$$F_{z_k}(z_k) = 1 - \exp \left( -\frac{z_k^2}{2\sigma_k^2} \right), \quad z_k \geq 0, \quad k = \{1, 2\}. \quad (10)$$

A comparison of joint and marginal distributions shows that the correlation between two detector outputs significantly complicates the expressions for the joint distributions. In spite of this algebraic complication, we would like to remind that the Marcum-Q and Bessel functions are readily available in many general-purpose computing programs and processed no more differently than the exponential function.

#### A. False Alarm and Threshold Calculation

The thresholds associated with both stages can be jointly selected to achieve a desired overall system false alarm probability. Remembering that the sole purpose of the first stage is to reduce the work load of the second stage, we suggest setting the threshold of the first stage in relation with the desired amount of load reduction. For example, to achieve a 20 fold load reduction,  $P_{FA1}$  can be selected as 1/20.

The false alarm probability of the first stage can be written as  $P\{z_1 > \gamma_1\} = 1 - F_{z_1}(\gamma_1) = P_{FA1}$  where  $\gamma_1$  is the associated threshold. Using (10) the first threshold can be determined as follows, [8]:

$$\gamma_1 = \sqrt{-2\sigma_1^2 \ln P_{FA1}}. \quad (11)$$

The second threshold ( $\gamma_2$ ) is selected to meet the system false alarm probability ( $P_{FA5}$ ). The system false alarm probability can be written as follows:

$$\begin{aligned} P\{z_1 > \gamma_1, z_2 > \gamma_2; H_0\} &= 1 - F_{z_1}(\gamma_1) - F_{z_2}(\gamma_2) + F_{z_1, z_2}(\gamma_1, \gamma_2) = P_{FA5}. \end{aligned} \quad (12)$$

The expressions for the joint and marginal cdf functions in the equation above are given in (8) and (10), respectively. When  $\gamma_1$  is substituted from (11) into this equation, we get the following

$$\begin{aligned} P_{FA1} &\left[ 1 - Q_1 \left( \sqrt{\frac{\gamma_2^2}{\sigma_2^2 (1 - \rho^2)}}, \sqrt{\frac{-2\rho^2 \ln P_{FA1}}{(1 - \rho^2)}} \right) \right] \\ &+ \exp \left( -\frac{\gamma_2^2}{2\sigma_2^2} \right) Q_1 \left( \sqrt{\frac{\rho^2 \gamma_2^2}{\sigma_2^2 (1 - \rho^2)}}, \sqrt{\frac{-2 \ln P_{FA1}}{(1 - \rho^2)}} \right) \\ &= P_{FA5}. \end{aligned} \quad (13)$$

This equation is to be solved for  $\gamma_2$  to achieve a desired system false alarm probability.

The left hand side of (13) is a monotonically decreasing function of  $\gamma_2$  and is lower bounded by zero. Hence  $\gamma_2$  value for which the equality is satisfied can be found by simple bisection methods. It should be noted that the other parameters appearing in (13) are given in (6) when  $\mathbf{R}_r$  is substituted with  $\mathbf{R}_{cn}$ .

#### B. Detection Probability Calculation

The expressions for the detection probability for Swerling-0 and Swerling-1 targets are presented. In the following section we numerically evaluate these expressions and compare the performance of the proposed system with the conventional system.

*Swerling-0 Targets:* This case corresponds to a nonfluctuating target with a fixed, nonrandom return power. For this case the parameter  $\alpha_s$  in (1) is taken as a constant. The signal-to-noise ratio (SNR) definition is  $\text{SNR} = |\alpha_s|^2 / \sigma_w^2$ , which is the SNR at the input of the clutter-suppressing filter.

Under hypothesis 1 the joint pdf of  $\hat{z}_1$  and  $\hat{z}_2$  is complex Gaussian distributed with the mean  $\alpha_s \mathbf{W}^H \mathbf{s}_\phi$  and the covariance matrix  $\mathbf{W}^H \mathbf{R}_{\text{cn}} \mathbf{W}$ . (The definition of  $\mathbf{W}^H$  and the definitions for  $\sigma_1^2$ ,  $\sigma_2^2$ ,  $\rho$  parameters are given in (5) and (6), respectively.) In addition we introduce  $m_k = |\alpha_s \mathbf{w}_k^H \mathbf{s}_\phi|$  for  $k = \{1, 2\}$ , which is the magnitude of the detector output in the absence of clutter and noise. The joint probability density of  $z_1$  and  $z_2$  can be written as follows, [9, p. 20]:

$$f_{z_1, z_2}(z_1, z_2) = \frac{z_1 z_2}{\sigma_1^2 \sigma_2^2 (1 - \rho^2)} \exp \left[ -\frac{1}{2(1 - \rho^2)} \left( \frac{z_1^2}{\sigma_1^2} + \frac{z_2^2}{\sigma_2^2} + \frac{m_2^2 \sigma_1^2 + m_1^2 \sigma_2^2 - 2\rho m_1 m_2 \sigma_1 \sigma_2}{\sigma_1^2 \sigma_2^2} \right) \right] \times \sum_{k=0}^{\infty} \epsilon_k I_k \left( \frac{z_1 z_2 \rho}{\sigma_1 \sigma_2 (1 - \rho^2)} \right) I_k \left( \frac{z_1 (m_1 - \rho m_2 \sigma_1 / \sigma_2)}{\sigma_1^2 (1 - \rho^2)} \right) I_k \left( \frac{z_2 (m_2 - \rho m_1 \sigma_2 / \sigma_1)}{\sigma_2^2 (1 - \rho^2)} \right) \quad (14)$$

where  $\epsilon_k$  is the Neumann factor. The Neumann factor is equal to zero for  $k = 0$  and is equal to 2 for other values.

The density given in (14) can be interpreted as the generalization of the well-known Rician distribution to two correlated random variables. The cumulative distribution function of this density is not available in closed form; hence the detection probability is numerically calculated by the probability integral  $P\{z_1 > \gamma_1, z_2 > \gamma_2; \mathbf{H}_1\} = \int_{\gamma_1}^{\infty} \int_{\gamma_2}^{\infty} f_{z_1, z_2}(z_1, z_2) dz_1 dz_2$ .

*Swerling-1 Targets:* This case corresponds to a fluctuating target that has a random return power at each burst. The random variable  $\alpha_s$ , given in (1), is independent of other random variables and has a circularly symmetric complex Gaussian distribution with zero mean and variance  $\sigma_s^2$ . The SNR definition for this case is  $\text{SNR} = \sigma_s^2 / \sigma_w^2$ , which is the ratio of average signal power and the average noise power at the input of the clutter-suppression filter.

Under hypothesis 1 the joint pdf of  $\hat{z}_1$  and  $\hat{z}_2$  is complex Gaussian distributed with zero mean and covariance matrix  $\mathbf{W}^H (\mathbf{R}_{\text{cn}} + \sigma_s^2 \mathbf{s}_\phi \mathbf{s}_\phi^H) \mathbf{W}$ . The detection probability calculation is similar to the false alarm probability calculation. The main difference is the substitution of  $(\mathbf{R}_{\text{cn}} + \sigma_s^2 \mathbf{s}_\phi \mathbf{s}_\phi^H)$  (instead of  $\mathbf{R}_{\text{cn}}$ ) for  $\mathbf{R}_{\text{r}}$  matrix in (6). The probability of detection for this case can be explicitly written as follows

$$P_d = P_{\text{FA}_1}^{1/(1+\text{SNCR}_1)} \left[ 1 - Q_1 \left( \sqrt{\frac{\gamma_2^2}{\sigma_2^2 (1 - \rho^2)}}, \sqrt{\frac{-2\rho^2 \ln P_{\text{FA}_1}}{(1 - \rho^2)(1 + \text{SNCR}_1)}} \right) \right] + \exp \left( -\frac{\gamma_2^2}{2\sigma_2^2} \right) Q_1 \left( \sqrt{\frac{\rho^2 \gamma_2^2}{\sigma_2^2 (1 - \rho^2)}}, \sqrt{\frac{-2 \ln P_{\text{FA}_1}}{(1 - \rho^2)(1 + \text{SNCR}_1)}} \right). \quad (15)$$

Here  $\text{SNCR}_1$  is the signal-to-clutter-and-noise ratio at the first detector output, which is  $\text{SNCR}_1 =$

$\sigma_s^2 |\mathbf{w}_1^H \mathbf{s}_\phi|^2 / (\sigma_c^2 \mathbf{w}_1^H \mathbf{R}_{\text{cn}} \mathbf{w}_1)$ . The other parameters appearing in (15) are calculated by setting  $\mathbf{R}_{\text{r}} = \mathbf{R}_{\text{cn}} + \sigma_s^2 \mathbf{s}_\phi \mathbf{s}_\phi^H$  in (6).

We note that when the threshold of the second stage is taken as zero, the two-stage detector is reduced to the single-stage detector, with the system false alarm probability of  $P_{\text{FA}_1}$ . The probability detection for this system can be found by substituting  $\gamma_2 = 0$  in (15). By using the relation  $Q_1(0, b) =$

$\exp(-b^2/2)$  in (15), the detection probability for this case can be found as  $P_d = P_{\text{FA}_1}^{1/(1+\text{SNCR}_1)}$ , which is the classical result for Swerling-1 targets, [8, p. 246]. We would like to note that the presented false alarm and detection probability relations for the two-stage detector contain the classical results for single-stage detectors and generalizes them to the cascade of two detectors.

### C. Computation Cost Calculation

The computational load of the first stage is determined by the MTI operation. The single line canceller has no multipliers and has the implementation cost of  $N - 1$  complex additions, where  $N$  is the number of pulses utilized in the coherent processing interval. The single-line canceller is followed by the fast Fourier transformation operation (FFT), which has the cost of  $O(N \log_2 N)$  additions and multiplications. The overall cost of this stage becomes as follows

$$\left( \begin{array}{l} \text{Computation Cost} \\ \text{1st Stage} \end{array} \right) : N - 1 + O(N \log_2 N) \text{ additions,} \\ O(N \log_2 N) \text{ multiplications.}$$

The computational cost of the second stage has two components: the cost for the construction of the linear combiner ( $\mathbf{w}_2 = (\sigma_c^2 \mathbf{R}_{\text{c}} + \sigma_w^2 \mathbf{I})^{-1} \mathbf{s}_\phi$ ) and

the cost of the inner product calculation ( $\mathbf{w}_2^H \mathbf{r}$ ). It should be noted that a new linear combiner should

be constructed for every Doppler steering vector  $\mathbf{s}_\phi$ , where  $\phi = 2\pi k/N$  and  $k = \{0, 1, \dots, N-1\}$ . Considering this, the overall cost becomes as follows

$$\left( \begin{array}{c} \text{Computation Cost} \\ \text{2nd Stage} \end{array} \right) : \left( \begin{array}{c} \text{Cost of Linear} \\ \text{Combiner Construction} \end{array} \right) \\ + (N^2 - N) \text{ additions,} \\ N^2 \text{ multiplications.}$$

The cost of inner product calculations is explicitly given in the right-most side of the presented relation. The cost of linear combiner construction is not specified since there can be a number of alternatives for its construction. For example, an offline calculation of  $\mathbf{w}_2 = (\sigma_c^2 \mathbf{R}_c + \sigma_w^2 \mathbf{I})^{-1} \mathbf{s}_\phi$  (for various clutter-to-noise ratios (CNRs) and for every  $\mathbf{s}_\phi$ ) and its storage in the system memory can be preferable for an implementation that has very limited computational resources. For this choice there is no cost in the calculation of the linear combiner. On the other hand, if online computation is feasible, the cost of linear-combiner calculation is  $O(N^3)$  multiplications for each  $\mathbf{s}_\phi$ , which is, in general, prohibitively high. Furthermore, adaptive radar systems can estimate the clutter covariance matrix from a set of neighboring cells in the vicinity of the cell of interest and then take the inverse of the estimated matrix. This operation is called the sample matrix inversion (SMI) [7]. For such systems the cost of covariance matrix estimation, which is  $O(LN^2)$ , adds on top of other costs. (Here  $L$  is the number of neighboring cells utilized in the covariance matrix estimation.) To summarize the cost of the second stage is at least  $O(N^2)$  due to inner product calculations and can be much more costly depending on that particular system.

A numerical comparison of the computational costs shows that the second stage is significantly more costly to run than the first stage when  $N > 16$ , which is the case for medium or high pulse-repetition-frequency (PRF) systems. A simple calculation shows that the suggested detector is advantageous to implement, i.e., the implementation cost of both stages is less than the implementation cost of the single stage with the optimal detector if  $P_{FA_1} < 1 - \text{Cost (Stage 1)}/\text{Cost (Stage 2)}$ . Hence, if the cost of the first stage is 90% of the second stage, then we can have a reduction in the implementation cost by selecting  $P_{FA_1}$  lower than 0.1. (The performance degradation brought by this choice, in terms of detection probability, is examined in the next section.) Furthermore, it should also be remembered that MTI operation, i.e., single line canceller followed by FFT, can be very efficiently implemented using standard field-programmable gate array (FPGA) libraries, therefore, the cost of engineering labor in the design and implementation of the first stage is also minimum.

### III. NUMERICAL RESULTS

The two-stage detector is not the optimal Neyman-Pearson detector; therefore it is expected to have a loss of detection probability at a fixed false alarm rate. In this section we quantify this loss and discuss whether the computation load reduction and other benefits brought by the two-stage detector can compensate the loss or not.

*Scenario:* A pulse Doppler surveillance radar with a rotating antenna making 20 r/min is transmitting 16 pulses at a burst. The system has a 20-element antenna array for elevation angle estimation. The azimuth beam pattern of the antenna is taken in the form of Gaussian shape with 3 dB beamwidth of 4 deg. The clutter is assumed to be mainly affected by the antenna scanning modulation. Under these conditions the clutter auto-correlation sequence can be written as  $r_c(k) = \sigma_c^2 \rho_c^{k^2}$ . The numerical value for the parameter  $\rho$  can be calculated as  $\rho_c = 0.998$ .

The target is assumed to have an SNR of  $-10$  dB and the CNR is fixed to 30 dB. The SNR value refers to the SNR before the beamforming, therefore it is the SNR at every receiver element (after the implementation of the pulse matched filter). If the array is steered exactly in the elevation direction of the target, then the SNR after beamforming is increased by 20 (13 dB). The system operates at the overall false alarm probability of  $10^{-5}$ .

*Swerling-0 Targets:* Figure 3 shows the probability of detection curves for the optimal Neyman-Pearson detector and the proposed two-stage detector. The detection probability is given for different target Doppler frequencies by varying the phase of the steering vector given in (2). The detection probability of the two-stage detector is given for  $P_{FA_1} = \{10^{-1}, 10^{-2}, 10^{-3}, 10^{-4}\}$  at the system false alarm probability of  $P_{FA_5} = 10^{-5}$ . Figure 3 shows that the loss in the probability of detection is negligible for  $P_{FA_1} = 10^{-1}$  and can be tolerated up to  $P_{FA_1} = 10^{-2}$ . The loss is quite significant for other  $P_{FA_1}$  values.

*Swerling-1 Targets:* Figure 4 presents the same comparison for Swerling-1 targets. Similar to the Swerling-0 case, the loss is negligible for  $P_{FA_1} = 10^{-1}$  and can be tolerable up to  $P_{FA_1} = 10^{-2}$ .

The presented probability of detection curves confirm the conceptual picture given in Fig. 2, which shows the first stage almost covers the region of the optimal detector when its false alarm probability is  $10^{-1}$ . For other  $P_{FA_1}$  values some of the probability mass contributing to the overall detection probability is discarded by the first stage and that loss is not recoverable by the second stage.

*Comments on Computational Load and Communication Data Rate Reduction:* As discussed in earlier sections, modern systems have the capacity of implementing some parts of the processing chain (such as matched filtering, beamforming) at the

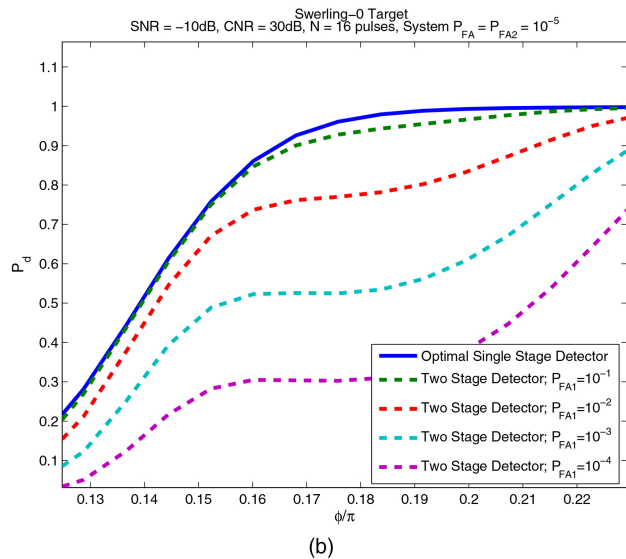
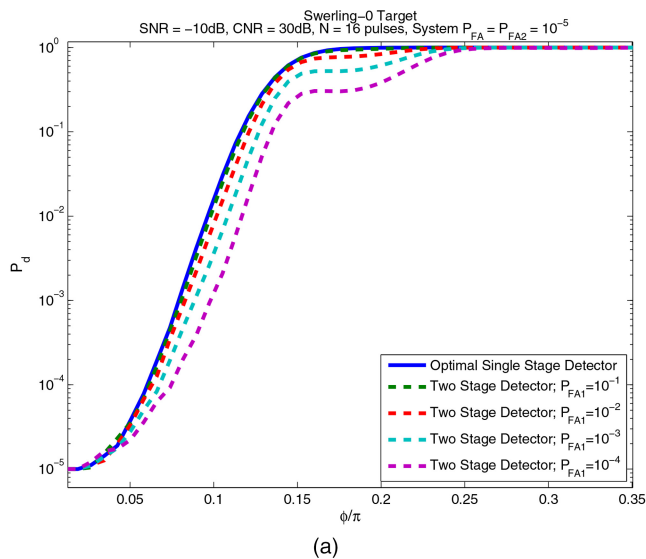


Fig. 3. Probability of detection comparison for proposed and optimal detector for Swerling-0 targets. Fig. 3(b) is zoomed version of Fig. 3(a) showing waterfall region.

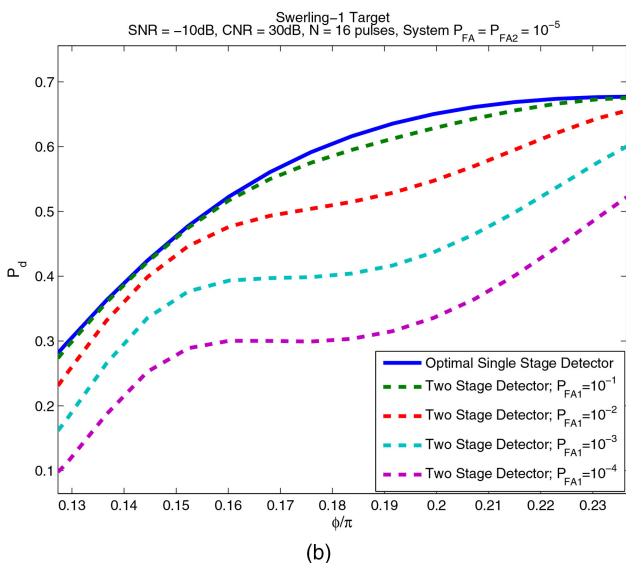
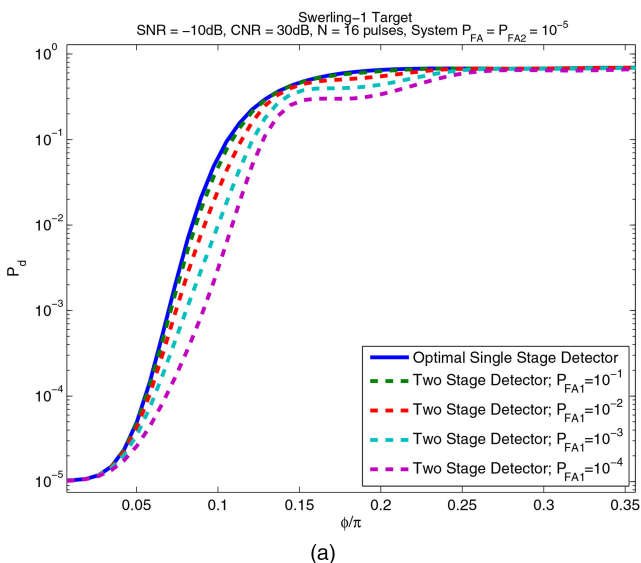


Fig. 4. Probability of detection comparison for proposed and optimal detector for Swerling-1 targets. Figure 4(b) is zoomed version of Fig. 4(a) showing waterfall region.

antenna unit. For the examined radar system, the output of the processing at the rotary antenna unit can be transferred to the central processing unit through the opto-mechanical components called slip rings. By implementing the first stage at the antenna unit, it is possible to reduce the amount of data transmission through the opto-mechanical device. For example, a choice of  $P_{FA1} = 1/20$  leads to a 20-fold communication data rate reduction and, at the same time, a 20-fold work-load reduction for the main processor. Such a large reduction in the requirements with a little performance loss is highly desirable, especially for high resolution systems.

*Further Comments on Load Reduction:* Figures 3 and 4 are generated with the assumption that

the elevation beam is steered towards the target direction, that is, an SNR gain of 20 is realized by beamforming. To further reduce the computational load, one may choose to have fewer beams covering the elevation sector of interest. The disadvantage of fewer beams is the loss in the beamforming gain.

In Fig. 5 the same scenario is examined at  $P_{FA1}$  of  $1/20$  for different SNR gains due to partial beamforming. It can be noted from Fig. 5 that the partial beamforming gains of  $\{16, 18, 20\}$  have almost the same detection probability. (The worst case drop in the detection probability is around  $\phi = 0.19\pi$  and has a value in between 0.04 and 0.06.) If a reduction in beamforming gain is tolerable, i.e., a gain of 16 instead of 20, then the elevation beamwidth is

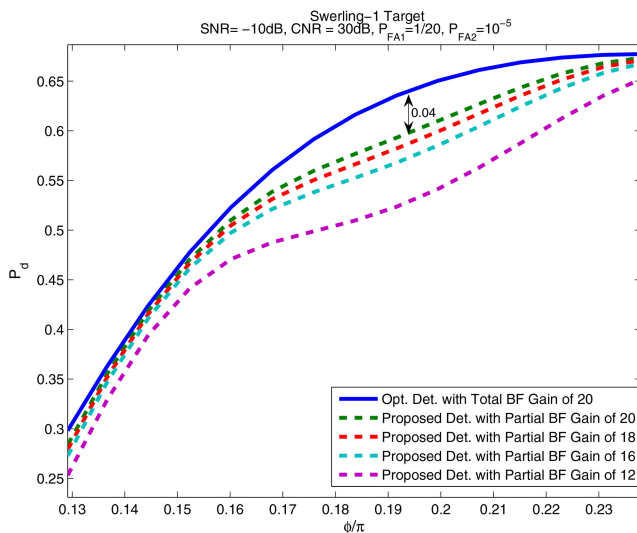


Fig. 5. Comparison of detection probabilities at different beamforming (BF) gains.

(roughly) increased by  $20/16 = 1.25$ , and the elevation sector of interest can be covered with less number of beams, which leads to an additional 20% savings in the computational cost.

**Comments on CFAR Operation:** The main disadvantage of the proposed system is the difficulty of calculating the constant false alarm rate (CFAR) threshold. Since the incoming cells are selectively transmitted to the second stage, there may not be a sufficient number of cells in the CFAR window to reliably estimate the detection threshold. A partial remedy can be the implementation of a clutter map in the first stage of the detector. The clutter map can be periodically transmitted to the second stage to assist the threshold calculation of the main detector to partially compensate for the absentee cells in the CFAR window.

#### IV. CONCLUSION

In this correspondence we present a reduced-complexity detection system with a minor loss in detection probability in comparison with the optimal system. The system operates by sifting the incoming data with a low-complexity detector first and then by presenting the sifted data to the scrutiny of the second detector. The goal is to discard some of the cells with little computational effort. We present the false alarm and the detection probability relations for the proposed detector and show that the proposed system leads to a significant reduction in computational complexity (on the order of 10 folds) and has a negligible loss in the detection probability if its parameters (threshold values) are properly selected.

A future work is the extension of the present study to non-Gaussian clutter distributions, especially to aid the detection process in sea clutter. The incorporation of CFAR to the presented system

is important and should be thoroughly examined. Lastly, the applicability of the proposed method in the resource management of multi-function radars can be examined [10].

ÇAĞATAY CANDAN

Department of Electrical and Electronics Engineering  
Middle East Technical University  
Ankara, TR-06530  
Turkey  
E-mail: (ccandan@metu.edu.tr)

#### REFERENCES

- [1] Farina, A. and Galati, G. Surveillance radars—State of the art, research and perspectives. *Alta Frequenza*, **4** (July–Aug. 1985), 261–267.
- [2] Watts, S., Baker, C., and Ward, K. Maritime surveillance radar. II. Detection performance prediction in sea clutter. *IEE Proceedings—F, Radar and Signal Processing*, **137**, 2 (Apr. 1990), 63–72.
- [3] Matthiesen, D. Efficient beam scanning, energy allocation, and time allocation for search and detection. *Proceedings of the IEEE International Symposium on Phased Array Systems and Technology (ARRAY)*, Waltham, MA, Oct. 12–15, 2010, pp. 361–368.
- [4] D’Addio, E., Farina, A., and Studer, F. Performance comparison of optimum and conventional MTI and Doppler processors. *IEEE Transactions on Aerospace and Electronic Systems*, **20**, 6 (Nov. 1984), 707–715.
- [5] Candan, C. and Yilmaz, A. Efficient methods of clutter suppression for coexisting land and weather clutter systems. *IEEE Transactions on Aerospace and Electronic Systems*, **45**, 4 (Oct. 2009), 1641–1650.
- [6] Gini, F., Farina, A., and Montanari, M. Vector subspace detection in compound-Gaussian clutter. Part II: Performance analysis. *IEEE Transactions on Aerospace and Electronic Systems*, **38**, 4 (Oct. 2002), 1312–1323.
- [7] Richards, M. A. *Fundamentals of Radar Signal Processing*. New York: McGraw-Hill, 2005.
- [8] Trees, H. L. V. *Detection, Estimation and Modulation Theory, Part 3*. Hoboken, NJ: Wiley, 1971.
- [9] Simon, M. K. *Probability Distributions Involving Gaussian Random Variables*. New York: Springer, 2006.
- [10] Miranda, S., et al. Knowledge-based resource management for multifunction radar: A look at scheduling and task prioritization. *IEEE Signal Processing Magazine*, **23**, 1 (Jan. 2006), 66–76.